Received: 13 August 2022 | Revised: 7 April 2023 | Accepted: 14 April 2023 | Published on: 28 May 2023

DOI: 10.1002/mrm.29689

RESEARCH ARTICLE

Magnetic Resonance in Medicine

A multiparametric alternative to short inversion-time inversion recovery for imaging inflammation: T_{2water} and fat fraction measurement using chemical shift–encoded turbo spin-echo MRI

Ruaridh M. Gollifer[1,2,3] | **Timothy J. P. Bray**[1,4] | **Ariona Kruezi**[2] | **Julia Markus**[1,4] | **Varvara Choida**[1,5] | **Margaret A. Hall-Craggs**[1,4] | **Alan Bainbridge**[2]

[1]Center for Medical Imaging, University College London, London, UK

[2]Department of Medical Physics and Bioengineering, University College London Hospital, London, UK

[3]Advanced Research Computing Center, University College London, London, UK

[4]Department of Imaging, University College London Hospital, London, UK

[5]Department of Rheumatology, University College London Hospital, London, UK

Correspondence
Timothy J. P. Bray, Center for Medical Imaging, University College London, London, UK.
Email: t.bray@ucl.ac.uk

Funding information
Action Medical Research; Albert Gubay Foundation, Grant/Award Number: GN2697; Humanimal Trust; NIHR Clinical Lectureship, Grant/Award Number: CL-2019-18-001; UCLH Biomedical Research Centre

Purpose: Short-inversion-time inversion-recovery MRI is used widely for imaging bone and soft-tissue inflammation in rheumatic inflammatory diseases, but there is no widely available quantitative equivalent of this sequence. This limits our ability to objectively assess inflammation and distinguish it from other processes. To address this, we investigate the use of the widely available Dixon turbo spin echo (TSE Dixon) sequence as a practical approach to simultaneous water-specific T_2 (T_{2water}) and fat fraction (FF) measurement.

Methods: We use a series of TSE Dixon acquisitions with varying effective TEs (TE_{eff}) to quantify T_{2water} and FF. The validity of this approach is assessed in a series of phantom and in vivo experiments, with reference values provided by Carr-Purcell-Meiboom-Gill acquisitions, MRS, and phantoms. The effect of inflammation on parameter values is evaluated in patients with spondyloarthritis.

Results: The T_{2water} estimates obtained from TSE Dixon were accurate compared with the reference values from Carr-Purcell-Meiboom-Gill and spectroscopy in both fat-free environments and in the presence of fat. FF measurements with T_{2water} correction from TSE Dixon were accurate from 0% to 60% FF and were not confounded by T_{2water} variations. In vivo imaging produced good quality images that were artifact free, produced plausible T_2 values, separating and quantifying the effect of inflammation on T_{2water} and FF.

Conclusion: The T_{2water} and FF measurements based on TSE Dixon with effective TE increments are accurate over a range of T_2 and FF values and could provide a widely available quantitative alternative to the short-inversion-time inversion-recovery sequence for imaging inflamed tissue.

KEYWORDS
inflammation, magnetic resonance imaging, radiology

Ruaridh M. Gollifer and Timothy J. P. Bray shared joint first authorship.
Margaret A. Hall-Craggs and Alan Bainbridge shared joint senior authorship.

1 | INTRODUCTION

Rheumatic inflammatory diseases are an interrelated group of conditions affecting the bones and joints of the skeleton. These diseases have two key features: inflammation (the response to harmful stimuli, which can also occur inappropriately in disease) and damage (defined as loss of structural or functional integrity of the tissue as a result of inflammation).[1] MRI has become a key component of pathways for diagnosing, phenotyping, and monitoring inflammation in rheumatic inflammatory diseases and is now used in standard care pathways in a number of diseases including spondyloarthritis, idiopathic inflammatory myositis, and juvenile idiopathic arthritis.[2,3,4,5] Additionally, MRI is used widely for imaging inflammation in other tissues, such as bowel, where the pathophysiology and imaging features share a number of common features with rheumatic diseases.[6]

Conventional MRI for the assessment of bone and soft-tissue inflammation in these diseases primarily relies on T_2-weighted short-inversion-time inversion-recovery (STIR) imaging. On STIR images, areas of hyperintensity indicate active inflammation, characterized by edema and cellular infiltration. The key biophysical mechanisms for this hyperintensity are thought to be an increase in proportional water content, with an accompanying reduction in fat content, and elongation of the T_2 of the water component (T_{2water}).[7,8–12] In the rheumatic inflammatory diseases, the identification of STIR hyperintensity is crucial for the detection of inflammation, and thus plays a key role in the patient pathway.

Although STIR images are used widely, they do have important limitations. First, the signal changes are nonspecific: Hyperintensity can occur in areas of inflammation but can also be caused by variations in normal marrow fat content, skeletal maturity, and inhomogenous fat suppression. Areas of increased fat content caused by fat metaplasia (a form of structural damage) can make interpretation difficult, because the presence of fat can "mask" modifications in water T_2 due to inflammation; additionally, areas of "spared" normal bone marrow are difficult to differentiate from edema/inflammation.[2,3] This limits assessment of inflammation in patients with coexisting inflammation and structural damage. Second, STIR images require qualitative interpretation, as there is no defined signal intensity threshold to differentiate normal from abnormal tissue.[13,14] Third, STIR images provide only imprecise assessment of change over time (partly as a result of the first and second issues, but also because of variations in slice thickness and scan geometry between scans), limiting assessment of response to treatment. This problem also limits the detection of structural damage, which accumulates slowly over time and can be difficult to detect and monitor using visual assessment alone.

Quantitative measurements of tissue characteristics could potentially disentangle the effects of inflammation from other processes (particularly those producing changes in fat content) and enable a more objective approach to tissue characterization. A number of approaches have been previously proposed, including the acquisition of Carr-Purcell-Meiboom-Gill (CPMG) sequences with a separate fat fraction (FF) acquisition used to constrain the fitting[15] and the use of T_2-prepared turbo spin-echo (TSE) imaging with spectral adiabatic inversion-recovery fat suppression.[16] A particularly attractive approach is the "IDEAL-CPMG" sequence,[11,12] which allows for simultaneous quantification of T_{2water}, T_{2fat}, and FF in a single acquisition; however, this sequence has several practical limitations and is not widely available, creating a barrier to implementation in clinical practice and multisite studies.

Here, we investigate the use of the widely available TSE Dixon sequence to separate and measure T_{2water} and FF. This method captures similar information to the STIR sequence but disentangles the processes and allows them to be separately quantified. By using a widely available sequence as a base, the proposed approach is intended to remove a barrier to translation into clinical practice and trials. Importantly, this method could provide images of diagnostic quality as well as quantitative data, as it has already been demonstrated that TSE Dixon (acquired at a single effective TE) can be used qualitatively as an alternative to STIR.[17]

2 | METHODS

2.1 | TSE Dixon sequence implementation

All experiments were performed on a 3T Philips Ingenia scanner. We quantify T_{2water} and FF using a series of TSE Dixon acquisitions, provided individually as a product by the manufacturer, with incrementally increasing effective TE (Figure 1).

First, TSE images are acquired with an effective TE (TE_{eff}) (Figure 1A). Next, the TSE acquisition is repeated with a small asymmetrical echo shift from the spin-echo position to facilitate fat-water separation (Figure 1B). Fat-water separation is achieved in-line on the scanner using a 2-point method[18]; however, the approach is not contingent on a particular method of fat-water separation. Finally, the first and second steps are repeated to yield fat-only and water-only images at a series of different TE_{eff} (Figure 1C,D).

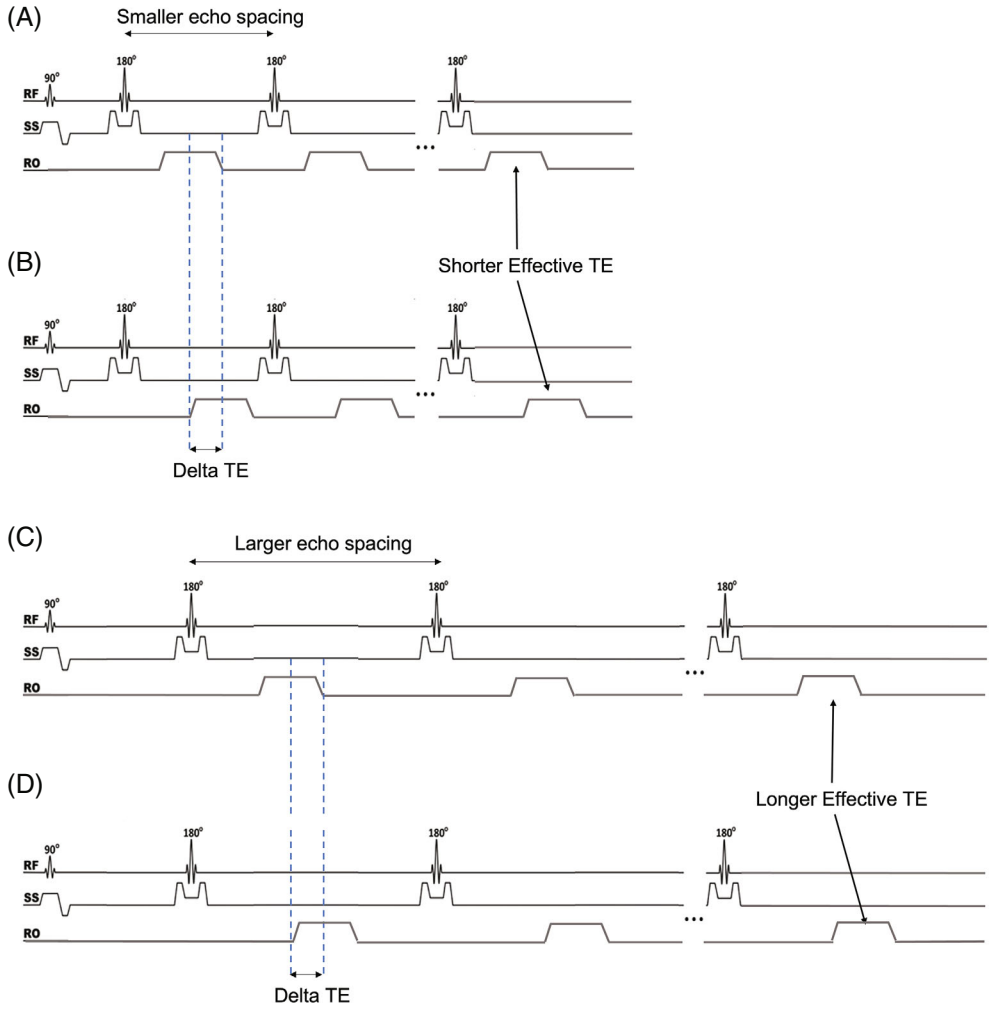

FIGURE 1 Sequence schematic of turbo spin-echo Dixon. There are two echoes acquired (shifted by ΔTE) for each effective TE acquisition. Examples are shown of the sequence for a shorter effective TE with a smaller echo spacing and ΔTE (A,B) and of the sequence for a longer effective TE with a larger echo spacing and ΔTE (C,D). The bandwidth remains fixed in both examples with the readout gradients being a constant height and duration. RO, readout; SS, single slice.

The mono-exponential decay curve is therefore fit across multiple effective TEs rather than across the echoes in a single echo train, as is the case with CPMG. This results in an "effective decay" curve with the true T_2 value if the inversion pulses in the CPMG train are precisely 180º, or a smooth, but slightly biased, effective decay curve with respect to the true T_2 value if the pulses are off resonance, which remains amenable to standard mono-exponential fitting (Figure 2).[19,20]

In the vendor-supplied implementation of the TSE Dixon acquisition, the receive bandwidth is usually automatically adjusted to optimize SNR for clinical imaging. For these experiments, the bandwidth was manually adjusted to be the same at each effective TE.

We obtained T_{2water} and T_{2fat} measurements using mono-exponential fitting of the water and fat signals at each TE_{eff}. This also yields estimates of the water and fat signals at $TE_{eff} = 0$, denoted as S_{0water} and S_{0fat} respectively. The FF is then calculated as follows:

$$FF = \frac{S_{0\ fat}}{S_{0\ fat} + S_{0\ water}} \quad (1)$$

FF estimations using TSE Dixon are therefore T_2-corrected, and the use of a long TR helps to minimize T_1 bias. However, because the method uses only two Dixon-encoded TEs, it may be susceptible to bias due to the spectral complexity of fat,[21] whilst B_1 inhomogeneity is also a source of bias.[22]

2.2 | Phantom experiments

Purpose-built phantoms were used to assess the ability of the TSE-Dixon methodology to quantify T_{2water} and FF by comparing with reference standard imaging methods and known reference values. In Experiment 1, T_{2water} values calculated using TSE Dixon were compared with T_{2water} values calculated using a CPMG sequence and STEAM spectroscopy in a T_2 phantom. In Experiment 2, the accuracy of the T_{2water} measurement was assessed in the presence of FF variations by comparing TSE Dixon with STEAM spectroscopy in a fat-water T_2 phantom. In Experiment 3, the accuracy of FF estimations was assessed in the presence of T_{2water} variations by comparing TSE Dixon with a vendor-supplied gradient echo–based proton

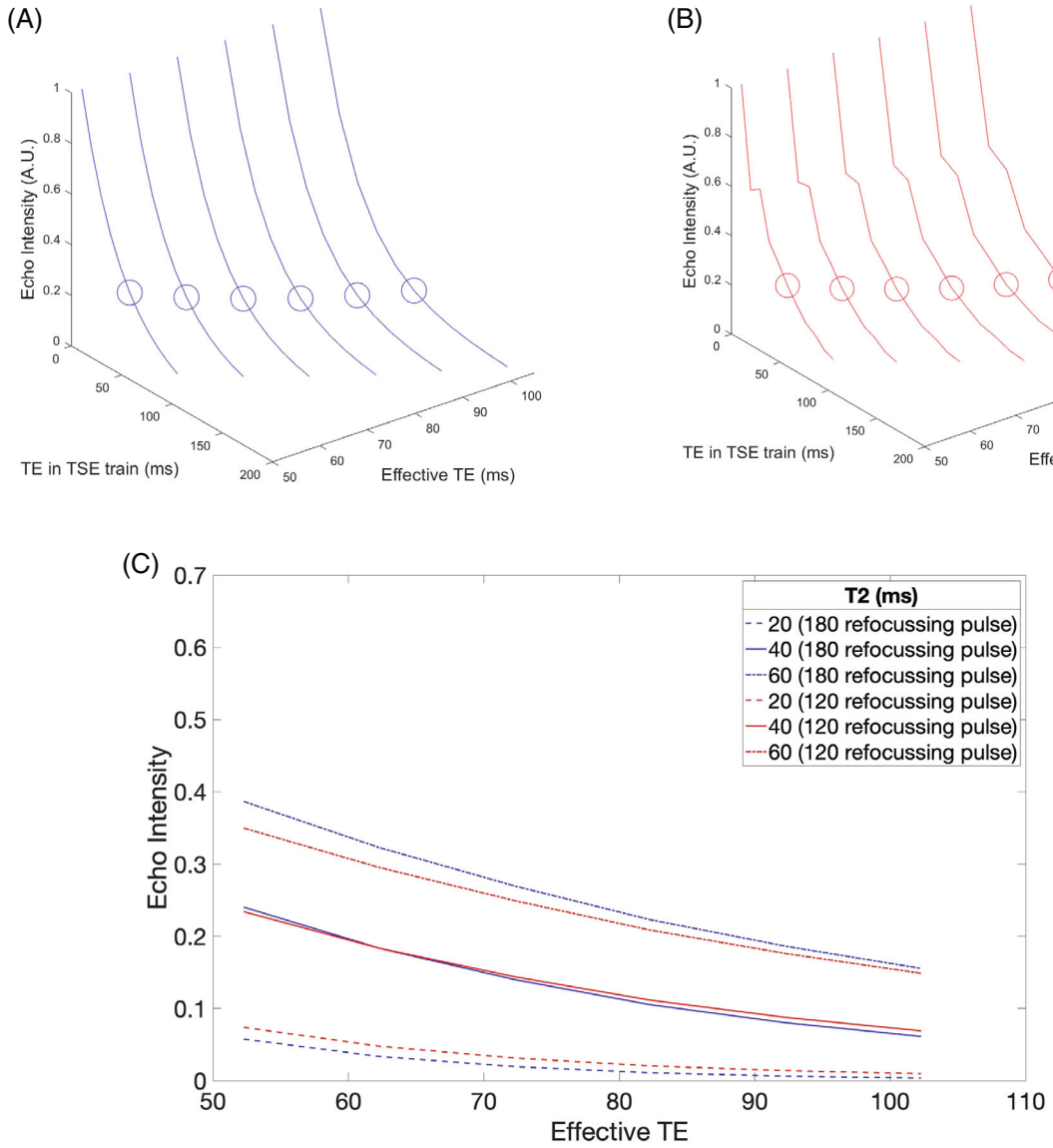

FIGURE 2 An example of extended phase graph (EPG) modeling of the turbo spin-echo (TSE) sequence. TSE trains for multiple effective TEs are shown for 180° (A, blue) and 120° (B, red) refocusing pulses for a T_2 value of 40 ms with the middle echo of each TSE train highlighted. The resulting decay curves across multiple effective TEs are used for the T_2 estimation for 180° and 120° (C) with T_2 values of 40 ms (solid line), 20 ms (dashed line), and 60 ms (dashed and dotted line).

density fat fraction (PDFF) quantification method and known fat concentrations in the same phantom.

To reduce the T_1 and T_2 contrast differences between the Dixon TSE, CPMG, and STEAM sequences, the same TR and similar TE scheme was used for each method. Specifically, the CPMG spin-echo spacing ranged from 10.3 ms to 116.9 ms to match the TSE Dixon TE scheme as closely as possible (effective TEs from 20 to 100 ms) and STEAM data were acquired with incrementally increasing TEs to match the Dixon TSE acquisitions (TE = 20, 30, 40, 60, 80 and 100 ms). A long TR (10 s for phantom and 5 s for in vivo data) was used to minimize the effect of T_1 weighting.[11]

2.2.1 | Phantom construction

Phantom 1 (fat-free gel T_2-varying phantom) was a Eurospin TO5 test object (Livingston, UK) with eight T_1 & T_2 Gel inserts (Leeds Test Objects, Leeds, UK) selected to provide a range of T_2 values.

Phantom 2 (fat-free pure agar T_2-varying phantom) was constructed in house and consisted of three containers with 2%, 3%, and 4% wt/vol agar (Sigma-Aldrich, St. Louis, Missouri, USA) solutions. Each batch of agar was heated before being added to each container and left to cool at room temperature to form the final solid gel phantom.

Phantom 3 (FF-T_2 varying phantom) was constructed in house and consisted of nine containers, each an emulsion with a different combination of agar concentration (2%, 3%, and 4% to vary T_{2water}[22]) and FF (using peanut oil, 20%, 40%, and 60% by volume). Peanut oil was used, as it has a lipid peak composition similar to human adipose tissue[20,23] with 55% oleic, 27% linoleic, 9% palmitic, and 4% stearic acids.[24] For each container, the necessary volume of peanut oil was measured out by weight, assuming the density of peanut oil (0.916 g/cm^3). Sodium dodecyl sulphate (surfactant; Sigma-Aldrich) was added to the peanut oil and gently mixed to form an initial emulsion, ensuring a final sodium dodecyl sulphate concentration in the mixture of approximately 30 mM. The 2%, 3%, and 4% wt/vol agar solutions were heated before being added to each container. The materials in each container were mixed and left to cool at room temperature to form the final solid gel phantom.

2.2.2 | Experiment 1 (T_{2water} estimation in fat-free environments)

Experiment 1 aimed to assess the accuracy of the T_{2water} measurements in the absence of fat using CPMG and STEAM MRS as a reference standard. Phantoms 1 and 2 were imaged using (1) the TSE Dixon sequence (as described previously; TR = 10 000 ms; 6 acquisitions; TE = 20, 30, 40, 60, 80, and 100 ms with echo spacing = 9.2, 13.8, 18.4, 27.6, 36.8, and 46 ms, respectively; ΔTE for Dixon encoding = 1 ms; echo-train length = 8; single 5-mm slice, excitation/refocusing angles 90º/180º; linear k-space ordering; half-scan factor = 0.6; bandwidth = 273.5 Hz; SENSE factor = 2; acquisition duration = 140 s per TE_{eff}, total of 840 s) and (2) a 2D CPMG sequence (Philips product sequence; TR = 10 000 ms; TE = 10 + n*3.4 ms with 32 echoes; single 5-mm slice, excitation/refocusing angles 90º/180º; acquisition duration = 1150 s). For the TSE Dixon processing (performed in-line on the scanner), the expected chemical shift difference for the lipid peaks relative to the water peak was modified to account for the temperature of the phantom being at room temperature rather than body temperature.[15,25]

Regions of interest (ROIs) were placed on the source Dixon TSE data water-only images and the CPMG data at each TE. The mean signal intensity at each TE was measured for each vial/container in the phantoms.

Single-voxel STEAM MRS was performed using a 3T Siemens MAGNETOM Vida scanner (10 × 10 × 10 voxels; TR = 10 s; 6 acquisitions; TE = 20, 30, 40, 60, 80, and 100 ms; bandwidth = 1.2 kHz; complex data points = 1024; number of averages = 2; mixing time = 10 ms). Note that this scanner was different than the scanner used for the TSE Dixon, as it generated better quality spectra. STEAM was chosen over PRESS to allow for shorter TE acquisitions and to account for J-coupling in fat.[26]

The MRS data were analyzed using AMARES[26] as implemented in the jMRUI[27,28] software package. Nine Gaussian peaks were used to cover the whole spectrum between 6 ppm and 0 ppm. The uncorrected water peak (i.e., the water peak at approximately 4.65 ppm, plus hidden fat peaks at approximately 5.4 ppm and 4 ppm) was calculated from the summation of individual peaks and the process repeated for the uncorrected or visible fat peaks (approximately 0.9, 1.3, 2.0, and 2.2 ppm). The proportion of fat peaks hidden under the water peak was estimated as 8.6% of the total fat signal, based on Hamilton et al.[29]

The final corrected water and fat peak signals were calculated as follows:

$$c\text{Water}_{\text{peak signal}} = \text{ucWater}_{\text{peak signal}} - h\text{Fat}_{\text{peak signal}} \quad (2)$$

$$c\text{Fat}_{\text{peaks signal}} = \text{ucFat}_{\text{peaks signal}} + h\text{Fat}_{\text{peak signal}} \quad (3)$$

where c = corrected, uc = uncorrected, and h = estimated hidden.

The value of T_{2water} from the MRS data was calculated for each container from the corrected water peak signals at each TE using a mono-exponential fit as described previously.

2.2.3 | Experiment 2 (T_{2water} estimation in presence of fat)

Experiment 2 aimed to assess the accuracy of T_{2water} estimation in the presence of fat using STEAM MRS as a reference standard in phantom 3. The 2D TSE Dixon sequence was implemented as for Experiment 1. Single-voxel STEAM MRS data were acquired as for Experiment 1.

2.2.4 | Experiment 3 (FF estimation)

Experiment 3 aimed to assess the accuracy of FF measurements obtained from TSE Dixon against those obtained from a quantitative PDFF measurement. Phantom 3 was imaged using 2D Dixon TSE (as described previously). PDFF measurements were obtained using the Philips mDixon Quant package, consisting of a 3D multi-echo spoiled gradient-echo sequence with bipolar readout gradients and with 6 echoes (TR = 7.8 ms; TE/echo spacing = 1.24/1 ms; flip angle = 3º; 30 slices with thickness = 1.5 mm; acquisition duration = 50.3 s).

2.2.5 | Statistical analysis

The measured values using the two techniques were compared using linear regression with 95% confidence intervals (CIs) calculated for the slope and intercept and Bland-Altman analyses with the coefficient of variation, the mean difference, and the 95% limits of agreement (LOAs). For Experiment 1, the comparison was between T_{2water} measurements from TSE Dixon and CPMG and from TSE Dixon and MRS. For Experiment 2, the comparison was between T_{2water} measurements from TSE Dixon and MRS. For Experiment 3, the comparison was between TSE Dixon FF and generated PDFF maps from mDixon Quant. Additionally, both TSE Dixon FF and mDixon Quant PDFF were compared to reference FF values in the phantom using linear regression.

2.3 | In vivo imaging

Three subjects were imaged: 1 healthy volunteer (male, 24 years) and 2 patients with axial spondyloarthritis (both male; Patient 1, age 19 years; Patient 2, age 17 years). All participants gave informed written consent before imaging, and the study was conducted with ethical approval (Queen Square Research Ethics Committee, reference REC 15/LO/1475).

2.3.1 | Image acquisition

TSE Dixon was performed with the following acquisition parameters: TR = 5000 ms; 6 acquisitions with TE = 20, 30, 40, 60, 80, and 100 ms with echo spacing = 9.2, 13.8, 18.4, 27.6, 36.8, and 46 ms, respectively; ΔTE for Dixon encoding = 1 ms; echo-train length = 8; single 5-mm slice; k-space ordering = linear; half-scan factor = 0.6; bandwidth = 273.8 Hz; SENSE factor = 2; and acquisition duration = 80–120 s per TE_{eff}, total of 480–720 s.

PDFF measurement was performed using the Philips mDixon Quant package, consisting of 3D multi-echo spoiled gradient-echo acquisition: 6 echoes; TR = 8.2 ms; TE/echo spacing = 1.47/1 ms; flip angle = 3º; 30 slices with thickness = 1.3 mm; and acquisition duration, 42.5 s.

CPMG was performed with the following parameters: TR = 5000 ms; TE = 10 + n*3.4 ms with 32 echoes; single 5-mm slice; excitation/refocusing angles = 90º/180º; and acquisition duration = 405–610 s.

T_2-weighted STIR was performed with TR = 5288/5316.4 ms; TE = 60 ms; TI = 210 ms; flip angle = 90°; 25 slices with 3-mm thickness; slice gap = 3.3 mm; and acquisition duration = 159 s.

Images were acquired in a modified coronal plane, parallel to the long axis of the sacrum.

2.3.2 | Healthy participant

The T_{2water} and FF maps were calculated from the TSE Dixon data, and FF maps were calculated from the PDFF data as described previously.

The TSE Dixon T_{2water} estimate was compared with the non-fat-suppressed CPMG T_2 estimate in the rectus femoris muscle of the volunteer and the muscle T_{2water} estimates from IDEAL-CPMG in literature.[11] In healthy tissue, muscle has a relatively low-fat content, so this allows the TSE Dixon T_{2water} estimate to be meaningfully compared with the CPMG T_2 estimate.[11] TSE Dixon was qualitatively compared with conventional STIR imaging by a consultant radiologist (7 years of experience of musculoskeletal MRI) to determine image quality. The criteria for this visual assessment were presence of artifacts, depiction of relevant anatomical structures, and whether the image was sufficiently clear for clinical interpretation.

To enable a fair comparison between the single TSE Dixon FF slice and mDixon Quant, the mDixon Quant PDFF map was averaged over multiple slices (because the mDixon Quant PDFF slices were thinner than the thicker TSE Dixon FF single slice). Linear interpolation was performed on an averaged mDixon Quant PDFF map to generate an image with the same matrix size as the TSE Dixon FF map using in-house software, written in *MATLAB*. An initial rigid registration was used to improve the accuracy of the registration, followed by affine registration to align the two maps. The difference between the registered mDixon Quant FF map and the TSE Dixon FF map was calculated to produce a difference FF map to compare the two methods.

2.3.3 | Patients with spondyloarthritis

To assess whether active inflammation could be detected using TSE Dixon imaging, 2 patients with extensive active sacroiliac joint inflammation (both with bone marrow edema, indicating active inflammation, and fat metaplasia, indicating damage, documented on a recent MRI and with clinical evidence of active disease according to symptom scores) were imaged.

To provide a qualitative assessment of the effect of pathology, the images were evaluated by a consultant radiologist (7 years of experience of musculoskeletal MRI) who evaluated the correspondence between signal abnormalities on the STIR image and changes in T_{2water}, S_{0water}, and FF on the parameter maps. To provide a quantitative assessment for Patient 1 of the effect of inflammation on parameter values, the consultant radiologist placed ROIs on the STIR image in regions of inflamed bone marrow (bone marrow edema), normal bone marrow, and fat

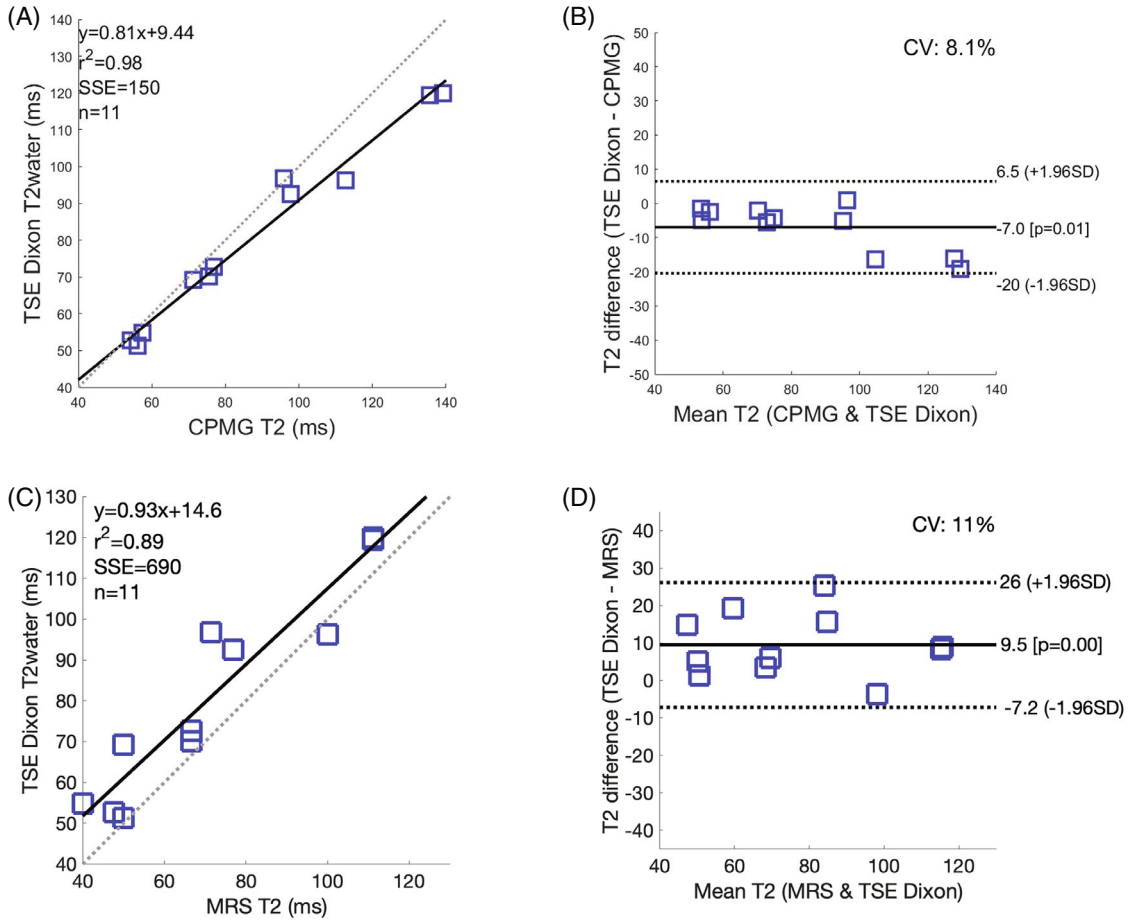

FIGURE 3 The T_{2water} estimates from TSE Dixon were linearly related to reference T_2 estimates from Carr-Purcell-Meiboom-Gill (CPMG) and MRS. (A–D) Linear regression (A,C) and Bland-Altman (B,D) comparison between TSE Dixon T_{2water} and CPMG T_2 (top) and TSE Dixon T_{2water} and MRS T_2 (bottom). Data from Phantoms 1 and 2 combined. CV, coefficient of variation; SSE, single-slice echo.

metaplasia. These ROIs were transferred to the water-only image for the first TE TSE Dixon acquisition, manually corrected for misregistration, and then automatically propagated onto the TSE Dixon T_{2water}, S_{0water}, and FF maps. The distribution of T_{2water}, S_{0water}, and FF values were compared between normal bone marrow (normal bm) and inflamed bone marrow (inflamed bm).

For Patient 2, linear regression and Bland-Altman analyses were calculated, as described previously, for FF estimates from TSE Dixon and mDixon Quant in various regions.

3 | RESULTS

3.1 | Phantom experiments

3.1.1 | Experiment 1 (T_2 estimation in fat-free environments)

The T_{2water} estimates from TSE Dixon were linearly related to reference T_2 estimates from CPMG (Figure 3A,B) and T_2 estimates from MRS (Figure 3C,D). For linear regression, the regression slope (95% CI) was 0.81 (0.73–0.90) and the regression intercept was 9.44 (1.70–17.19) for the CPMG comparison, and the regression slope (95% CI) was 0.93 (0.72–1.1) and the regression intercept was 14.6 (−1.6 to 30.7) for the MRS comparison. For the Bland-Altman LOA analysis, the mean difference was −7.0 ms and the 95% LOAs were −20 to 6.5 ms for the CPMG comparison, and the mean difference was 9.5 ms and the 95% LOAs were −7.2 to 26 ms for the MRS comparison.

3.1.2 | Experiment 2 (T_2 estimation in the presence of fat)

The T_{2water} estimates from TSE Dixon were linearly related to reference T_2 estimates from MRS over the range of FF concentrations investigated (Figure 4). For linear regression, the regression slope was 0.87 (0.59–1.15), and the regression intercept was 9.76 (0.54–18.98). For Bland-Altman LOA analysis, the mean difference was 5.8

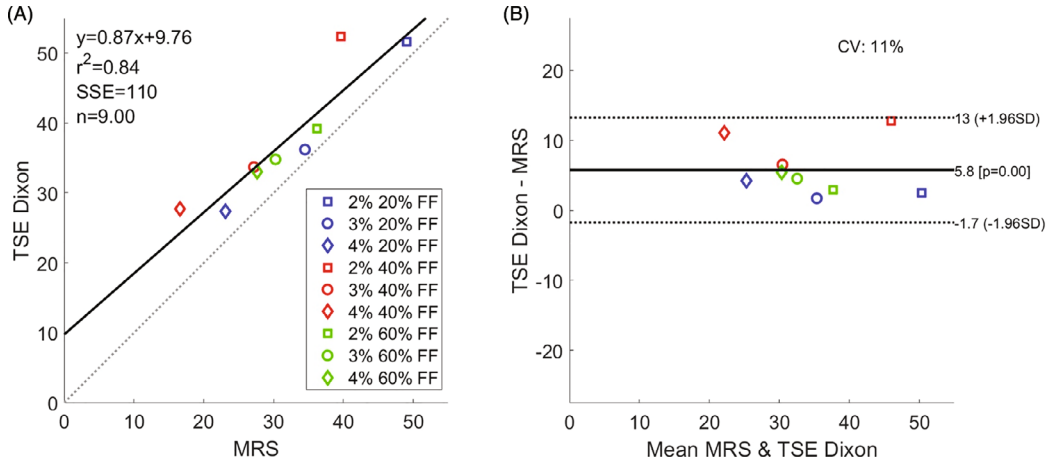

FIGURE 4 T_{2water} estimates from TSE Dixon were linearly related to reference T_2 estimates from MRS over the range of fat fraction (FF) concentrations. (A,B) Linear regression (A) and Bland-Altman (B) comparison between TSE Dixon T_{2water} and MRS T_{2water}. Data from Phantom 3 (blue, 20% FF; red, 40% FF; green, 60% FF; square, 2% agar; circle, 3% agar; diamond, 4% agar).

FIGURE 5 FF estimates from TSE Dixon were linearly related to proton density fat fraction (PDFF) estimates. (A,B) Linear regression (A) and Bland-Altman (B) comparison between TSE Dixon FF and PDFF FF. Data from Phantom 3 (blue, 2% agar; red, 3% agar; green, 4% agar).

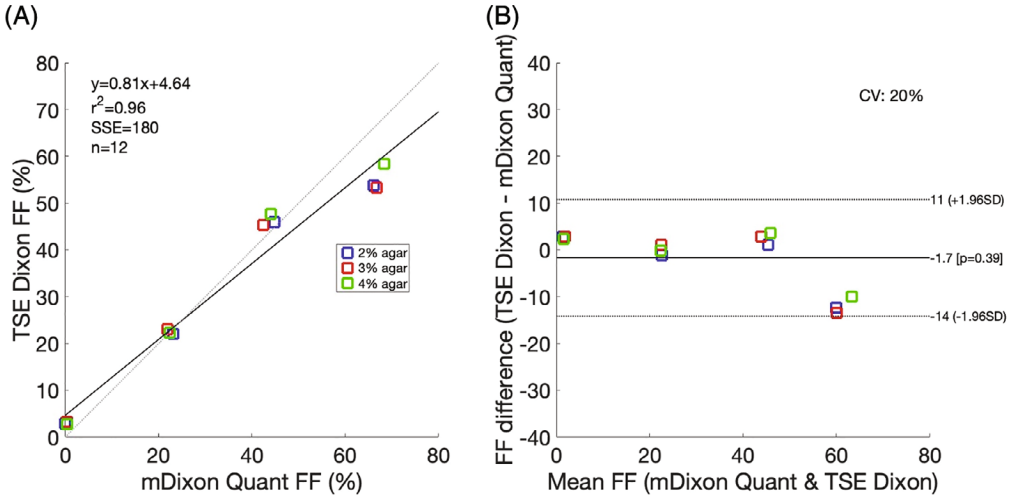

and the 95% LOAs were −1.7 to +13. The T_2 from TSE Dixon was longer than the T_2 from MRS T_2.

3.1.3 | Experiment 3 (FF estimation in presence of variable T_2)

FF estimates from TSE Dixon were linearly related to PDFF FF estimates (Figure 5). For linear regression, the regression slope was 0.81 (0.71–0.91) and the regression intercept was 4.64 (0.58–8.7). For the Bland-Altman LOA analysis, the mean difference was −1.7% and the 95% LOAs were −14% to 11%. The measured FF from TSE Dixon matched the reference FF from mDixon Quant closely for FF values of 0%, 20%, and 40% FF. For 60% FF, there was a larger difference between TSE Dixon FF and mDixon Quant FF.

For linear regression between TSE Dixon FF estimates and known FF, the regression slope was 1.07 (0.95–1.19) and the regression intercept was −4.08 (−8.64 to 0.47).

For linear regression between PDFF FF estimates and known FF from the phantoms, the regression slope was 0.90 (0.88–0.92) and the regression intercept was −0.11 (−0.90 to 0.68).

3.2 | In vivo imaging

3.2.1 | Healthy participant

The T_{2water}, S_{0water}, FF, and T_{2fat} maps derived from TSE Dixon sequences and the mDixon Quant PDFF map are shown in Figure 6A–D. The T_{2water} maps showed plausible values throughout all imaged structures with no significant artifact. As expected, the T_{2water} map showed consistent values less than about 60 ms throughout the whole bone marrow, with areas of higher T_{2water} observed in the neural foramina and intervertebral disc. These areas of higher T_{2water} corresponded closely to areas of higher signal on the STIR image. FF values were also

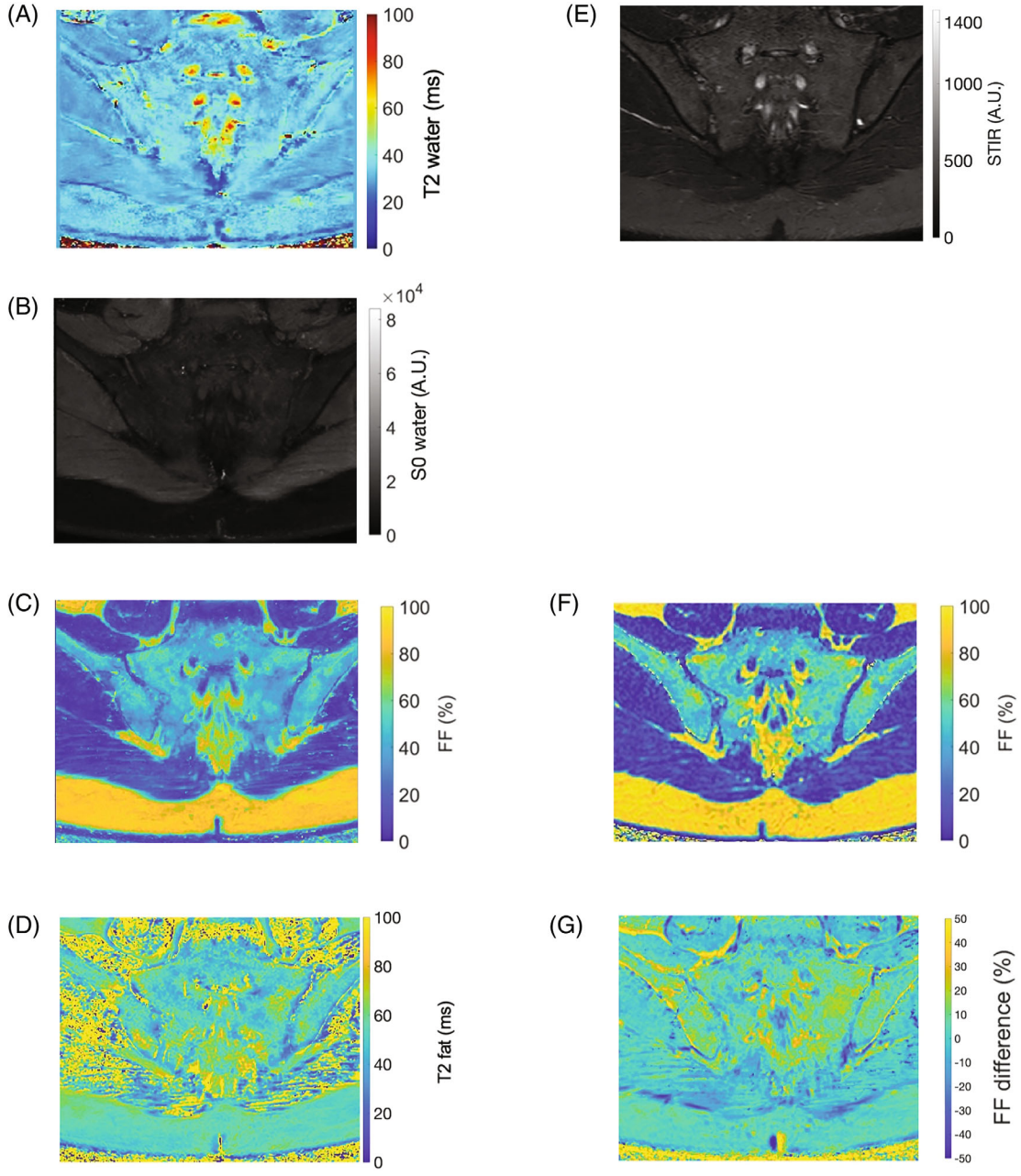

FIGURE 6 Healthy participant in vivo images showed plausible values across structures with varying T_2 and minimal image artifacts. T_{2water} (A) and S_{0water} (B) maps showed consistent values through the whole bone marrow, with a similar pattern to short-inversion-time inversion-recovery (STIR) images (E). The FF map derived from TSE Dixon sequences (C) and the PDFF mDixon Quant FF map (F) showed FF values in the bone marrows of 40%–60%. The FF difference map (G) demonstrated differences between the FF methods. Note that these differences are generally small, although some well-defined areas of greater differences arise in interfaces between tissues due to slight misregistration of the two scans. (D) The T_{2fat} map showed consistent values through the whole bone marrow.

plausible in all imaged structures (including subcutaneous fat, muscle, and bone marrow), with good qualitative agreement compared with the PDFF map. The FF difference map (compared against mDixon Quant) also showed minimal differences throughout most of the bone marrow (Figure 6C,F,G). The T_{2water} value from muscle was 29.9 ms, which corresponded closely with a previous literature estimate of 30 ms from IDEAL-CPMG,[11] whereas the non-fat-suppressed CPMG yielded a higher estimate of 42.2 ms.

3.2.2 | Patients with spondyloarthritis

The T_{2water}, S_{0water}, FF, and T_{2fat} maps derived from TSE Dixon sequences and the corresponding mDixon Quant

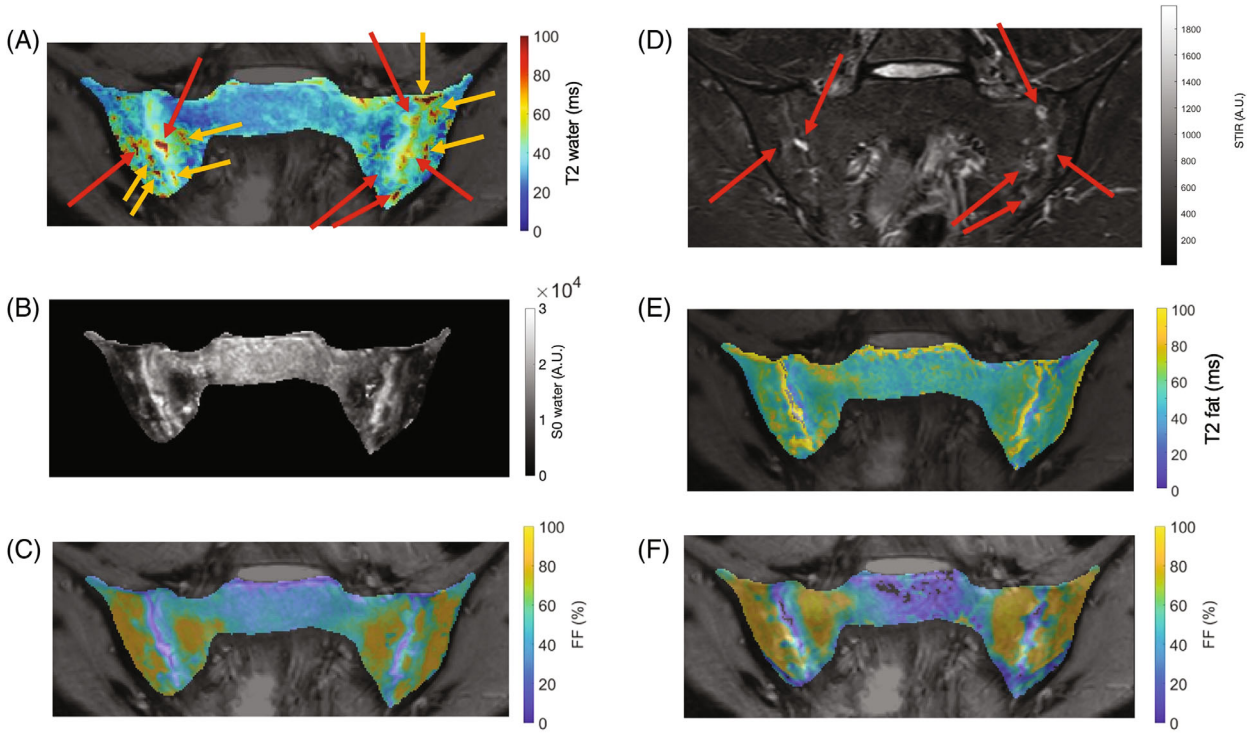

FIGURE 7 T_{2water} imaging can detect active inflammation (Patient 1). Active inflammation produces regions of increased T_{2water} (A, red arrows), corresponding to areas of hyperintensity seen on STIR imaging (D). There are additional areas of increased T_{2water} (yellow arrows) that may represent inflammation "missed" by the conventional STIR imaging and suggest a potentially greater sensitivity of T_{2water} compared with STIR signal intensity for imaging inflammation. (B) Corresponding increases in S_{0water} in areas of inflammation. (C) Extensively high FF in the subchondral bone marrow, in keeping with fat metaplasia being caused by previous inflammation. The overlap between these areas of fat metaplasia and the inflammation shown in (A) suggests that the T_{2water} map can detect inflammation even within areas of fat metaplasia (traditionally a confound on interpretation of STIR images). (F) The areas of increased fat content agree closely with those demonstrated on the gradient echo–based PDFF map. Some small discrepancies in the precise spatial distribution of the subchondral fat may relate to differences in slice thicknesses and/or movement between acquisitions. (E) The T_{2fat} shows areas of high T_2, although this is not closely associated with increased T_{2water}, suggesting that T_{2fat} is not greatly biasing the T_{2water}.

PDFF maps are shown in Figures 7 and 8 (Patients 1 and 2), and the corresponding parameter distributions obtained from the ROIs placed on regions of inflammation (for Patient 1) are shown in Figure 9. Active inflammation is seen as multiple focal areas of increased T_{2water} on the TSE Dixon T_{2water} maps, which correspond very closely to areas of hyperintensity on the STIR images. Interestingly, the regions of T_{2water} abnormality are more extensive than the corresponding areas of STIR abnormality, suggesting that this method may be capturing additional inflammation that is missed by the STIR image. The FF maps demonstrate areas of increased fat content in the subchondral bone marrow in keeping with fat metaplasia (i.e., increased marrow fat content caused by previous inflammation), which overlaps in distribution with the areas of inflammation.[4] Note that the increases in T_{2water} overlap with these areas suggest that the presence of fat does not obscure inflammation in the TSE Dixon T_{2water} map.

Figure 8 graphically demonstrates the increases in T_{2water} observed in areas of inflammation. Again, note that the FF was increased and S_{0water} was decreased in areas of inflammation, likely reflecting the presence of underlying fat metaplasia.

FF estimates from TSE Dixon were linearly related to PDFF FF estimates in Patient 2 (Figure 10). For linear regression, the regression slope was 0.77 (0.57–0.98) and the regression intercept was 10.9 (−1.3 to 23.1). For the Bland–Altman LOA analysis, the mean difference was 0.75% and the 95% LOAs were −22% to 21%.

4 | DISCUSSION

In rheumatic inflammatory diseases, active inflammation in the bone marrow manifests as regions of hyperintensity on STIR images, which may be attributed to some combination of increased T_{2water} and reduced FF.[7,11,12] STIR contrast changes are nonspecific; other processes can mimic or "mask" inflammation, and assessment is subjective and qualitative.[2,3,16] Similar difficulties can exist in

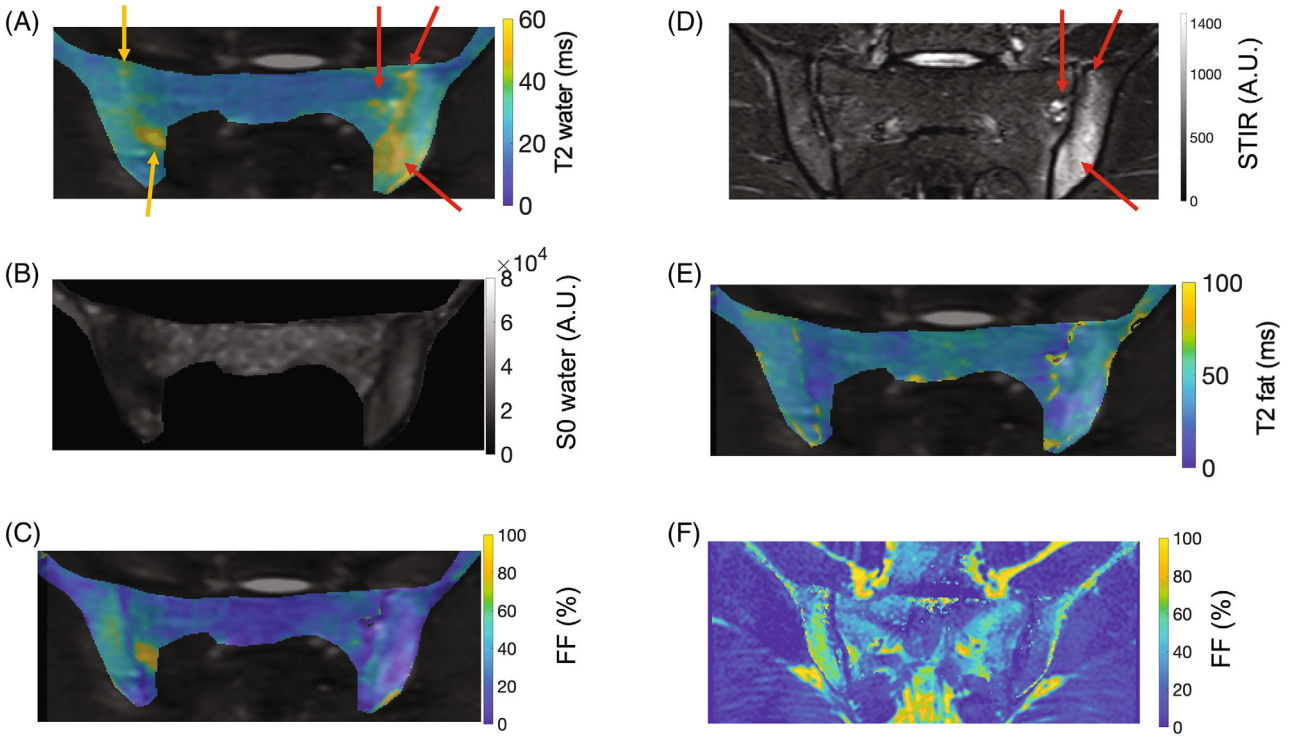

FIGURE 8 T_{2water} imaging can detect active inflammation (Patient 2). Active inflammation produces regions of increased T_{2water} (A, red arrows) corresponding to areas of hyperintensity seen on STIR imaging (D). Similar to Patient 1, there are additional areas of increased T_{2water} (yellow arrows in the subchondral bone, related to the right sacroiliac joint [SIJ]) that may represent inflammation "missed" by the conventional STIR imaging and suggest a potentially greater sensitivity of T_{2water} compared with STIR signal intensity for imaging inflammation. (B) Corresponding increases in S_{0water} in areas of inflammation. (C) Small areas of high FF in the subchondral bone marrow related to the right SIJ, in keeping with fat metaplasia caused by previous inflammation. Again, the overlap between these areas of fat metaplasia and the inflammation shown in (A) suggests that the T_{2water} map can detect inflammation even within areas of fat metaplasia (traditionally a confound on interpretation of STIR images). (F) The areas of increased fat content agree closely with those demonstrated on the gradient echo–based PDFF map.

inflammatory diseases affecting other tissues.[6] Here, we propose the use of TSE Dixon acquisitions with incrementally increasing effective TEs to separate or "disentangle" T_{2water} and FF, thus providing a more objective method for the assessment of inflammation, which is less prone to misinterpretation due to these overlapping processes.

When imaging inflammation, the simultaneous presence of fat and water in a tissue necessitates the separation of these signals before quantification. One approach to this problem, described by Janiczek et al., is known as IDEAL-CPMG. In this approach, asymmetric echoes are added to a CPMG echo train to allow separation of water and fat signals using the IDEAL algorithm.[11] The intention of this work was to take a similar approach, but to use a TSE Dixon sequence that is widely available from all the major MRI scanner manufacturers, and thus potentially facilitate use in clinical practice and trials.

The key results of our study are as follows. First, we showed that T_{2water} measurements using TSE Dixon were accurate across a range of physiologically relevant T_2 values and agreed closely with CPMG- and MRS-based estimates. There was a small bias between the methods, with TSE Dixon appearing to underestimate T_{2water} relative to CPMG at higher T_2 values, which could relate to imperfections in the TSE Dixon and/or CPMG sequences but was relatively small compared with the observed effect of inflammation in patients. Second, we showed that T_{2water} measurements using TSE Dixon were accurate in the presence of fat, with no significant confounding effect of varying FF. Although there was a small positive bias between MRS and TSE Dixon (which may be similar in origin to that mentioned previously), again this was relatively small compared with the biological effect size in question. Third, we showed that FF measurements obtained using TSE Dixon agreed closely with those obtained using a quantitative gradient echo–based method for PDFF measurement, suggesting that the TSE Dixon–based FF measurements could be a useful addition to the T_{2water} measurement. Fourth, we showed that TSE Dixon–based T_{2water} and FF maps demonstrated plausible values in vivo and minimal

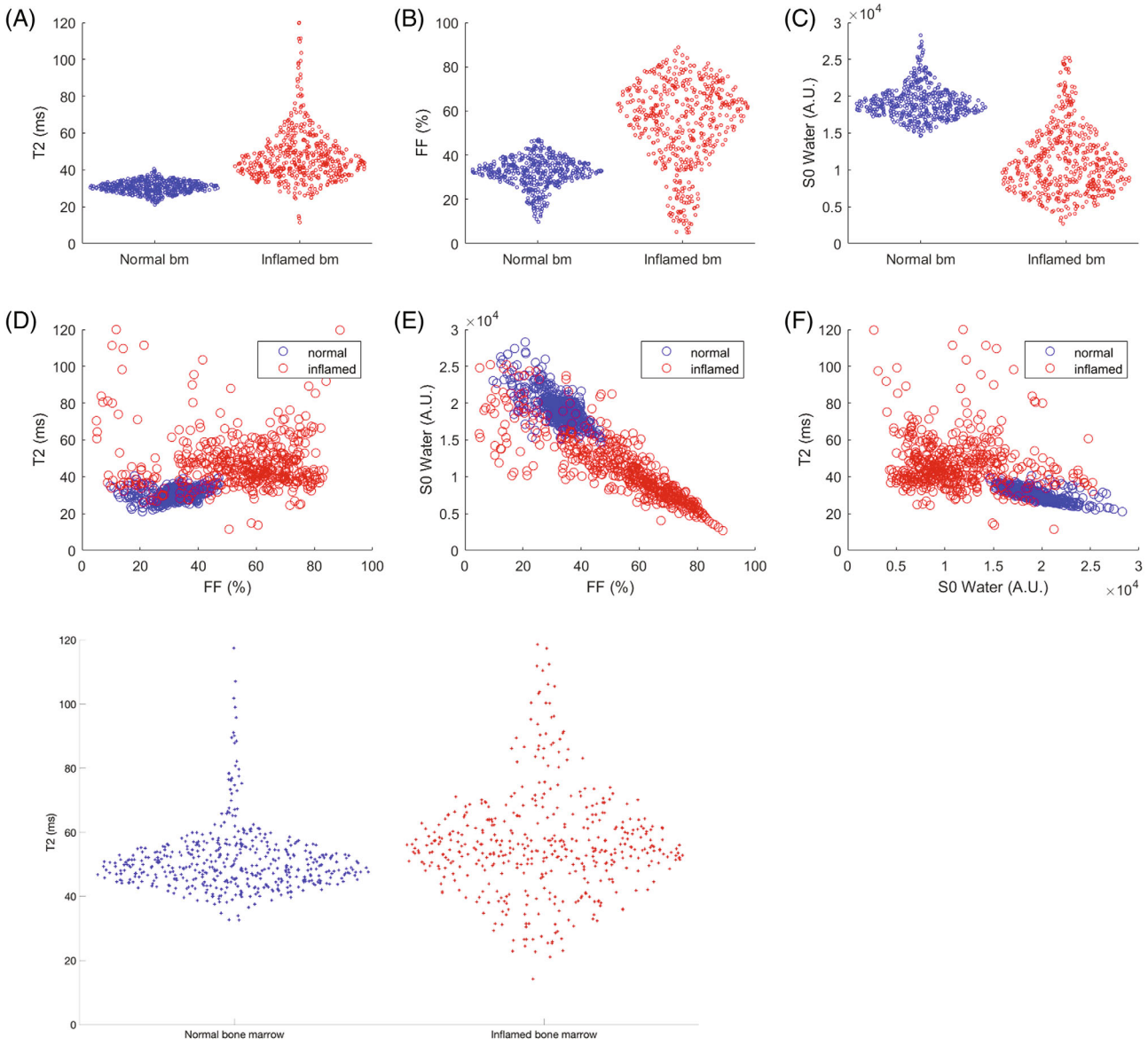

FIGURE 9 Distribution of T_{2water} (A), FF (B), S_{0water} (C), and T_{2fat} (G) values in normal bone marrow and inflamed bone marrow in Patient 1. Scatterplots of T_{2water} (D) versus FF, S_{0water} vs. FF (E), and T_{2water} vs. S_{0water} (F).

artifacts. Finally, in patients with spondyloarthritis, we demonstrated the feasibility of the technique for imaging inflammation: We observed increased T_{2water} values in areas of active inflammation, corresponding closely to areas of hyperintensity on STIR images. Interestingly, the regions of high signal intensity were more extensive on TSE Dixon T_{2water} images than on STIR, suggesting that T_{2water} measurements may be more sensitive to inflammation. If some regions of inflammation were indeed "missed" by STIR imaging, this could be explained by the fact that the FF was actually increased in much of the subchondral bone marrow, likely due to underlying fat metaplasia as a result of previous inflammation.[2] Further research is required to investigate the interplay between T_{2water} and FF in patients with pre-existing structural damage, but from a theoretical standpoint, our method should have a significant advantage over STIR imaging.

In general, for a simultaneous T_{2water} and FF sequence, incorporation of a series of spin echoes (to quantify T_2) with the additional collection of echoes with a small asymmetrical echo shift from the spin-echo position (to facilitate fat-water separation in quantifying T_{2water} and FF) is necessary. One approach, known as IDEAL-CPMG, whereby a CPMG sequence was modified to incorporate additional collection of gradient echoes about each spin echo in the CPMG train (thus enabling fat-water separation for each spin echo), was described by Janiczek et al.[11,12] Our TSE Dixon approach is somewhat similar, with each acquisition consisting of a series of spin echoes and an echo with an asymmetrical echo shift to

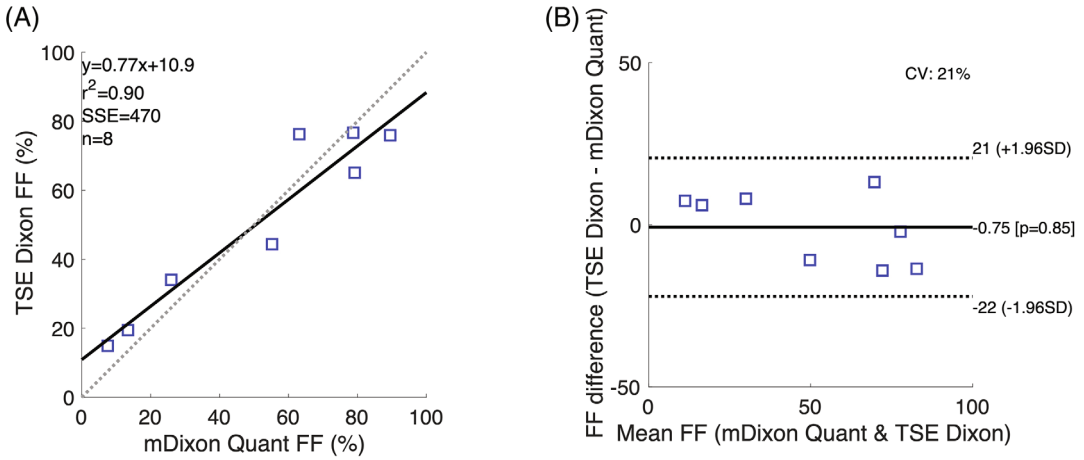

FIGURE 10 FF estimates from TSE Dixon were linearly related to reference FF estimates from mDixon Quant in various regions. (A,B) Linear regression (A) and Bland-Altman (B) comparison between TSE Dixon FF and mDixon Quant FF.

facilitate fat-water separation. However, we used multiple TSE Dixon acquisitions to yield fat-only and water-only images at a series of different TE_{eff}, to enable T_{2water} and FF quantification. Our approach has several potential advantages over IDEAL CPMG. First, the TSE Dixon method can easily be implemented on all major vendors to enable reproducible research, clinical translatability, and potential use in multicenter studies. Second, TSE Dixon may be substantially more flexible and time-efficient than IDEAL-CPMG, as any number of arbitrary TE_{eff} can be collected without introducing "dead time" into the acquisition, whereas this is not the case for IDEAL-CPMG. For example, it would be entirely possible to efficiently collect only two values of TE_{eff} (e.g., short and long) with a TSE Dixon method, whereas with IDEAL-CPMG this would result in substantial dead time in the middle of the acquisition, meaning that the total acquisition time might not be reduced. This advantage of TSE Dixon over IDEAL-CPMG can be "traded in" to improve spatial resolution, which is an important requirement for a method used to image a spatially heterogenous process where regions of abnormalities are often small. The greater flexibility of TSE Dixon could also allow for very closely spaced echoes, potentially of value when imaging short T_2 species and for multicompartment modeling, whereas this is limited in IDEAL-CPMG by the duration of the (typically unipolar) readout gradients.[11] Third, the fitting with CPMG has the added complexity that stimulated echoes directly manifest themselves as fluctuations in echo intensity over the early echoes, which is circumvented by using TSE Dixon. Finally, the original implementation of IDEAL-CPMG required manual seed point placement in combination with a region-growing algorithm to achieve fat-water separation, whereas this is avoided with our method.

This study has several limitations. First, the agreement of TSE Dixon T_{2water} estimates with the reference methods was linear, but with some observable biases. It is likely that undesirable stimulated echoes within the TSE Dixon echo train, occurring as a result of B_1 inhomogeneity,[21] are affecting the quantification of T_{2water}. Approaches to correct for the presence of stimulated echoes include discarding some echoes from the fit,[30] using a linear correction scheme,[31] using the extended phase graph to model the acquisition,[21,32-34] or using a dictionary-based method.[35-37] Applying one of these approaches may further improve the accuracy of the method. Second, the length of the Dixon TSE acquisitions was longer than desirable, reflecting the fact that the TSE Dixon was acquired with a relatively "rich" acquisition scheme using high spatial resolution, multiple effective TEs, and a long TR to minimize T_1 weighting, to ensure sufficient quality for this validation study. In practice, all these factors could potentially be reduced, resulting in a scan time similar to or less than STIR in clinical practice. Further work could focus on optimization of the number and timing of individual echoes, development of a T_1-bias adjustment scheme to allow shortening of the TR, and acceleration using parallel imaging and compressed sensing. Third, with TSE imaging, the images can be susceptible to blurring, as the k-space data for a particular effective TE are actually collected at a range of actual TE, and this typically worsens when longer effective TEs are used. However, the blurring is no more severe than with conventional TSE imaging, which is typically deemed acceptable for and widely used in clinical practice. Fourth, for the longer effective TEs, the TSE echo spacing was large with only a few milliseconds actually used for the data acquisition. Potential future work could involve finding ways to fill in this dead space, to make the sequence more efficient. Importantly, the method has the potential

to save time in a clinical setting, as it provides both inflammatory and structural information[3] and could therefore remove the need for multiple acquisitions (conventionally STIR and T_1-weighted spin-echo imaging in one or two planes each) to assess these features. In the future, it would also be of value to explore other, related methods such as MR fingerprinting, which has recently been shown to be capable of FF, as well as T_1 and T_2 estimation.[38,39] Ultimately, the choice of sequence will be dictated by some tradeoff of speed, image quality (including spatial resolution and artifacts), and quantification accuracy. Fifth, although the 20% and 40% Dixon TSE FFs corresponded closely with the reference standard FF, there was some discrepancy with the 60% FF due to the difficulty in mixing the oil and agar. This may also have affected the results with the T_2 values at 60% FF. Finally, the in vivo evaluation provided here is preliminary; further study is needed for detailed biologic validation and to assess clinical efficacy compared with existing techniques.

5 | CONCLUSIONS

The proposed T_{2water} and FF measurements, based on TSE Dixon with TE_{eff} increments, are accurate over a range of T_2 and FF values and could provide a widely available quantitative alternative to the STIR sequence for imaging inflamed tissue. Our results suggest that the proposed methodology is promising and warrants further development and evaluation in larger studies.

ORCID

Ruaridh M. Gollifer https://orcid.org/0000-0001-9319-936X
Timothy J. P. Bray https://orcid.org/0000-0001-8886-5356
Margaret A. Hall-Craggs https://orcid.org/0000-0001-8734-4065

TWITTER

Timothy J. P. Bray @tjp_bray

REFERENCES

1. Walsh NC, Crotti TN, Goldring SR, et al. Rheumatic diseases: the effects of inflammation on bone. *Immunol Rev*. 2005;208:228-251. doi:10.1111/J.0105-2896.2005.00338.X
2. Sieper J, Rudwaleit M, Baraliakos X, et al. The assessment of Spondyloarthritis International Society (ASAS) Handbook: a guide to assess spondyloarthritis. *Ann Rheum Dis*. 2009;68:ii1-ii44. doi:10.1136/ard.2008.104018
3. Bray TJP, Jones A, Bennett AN, et al. Recommendations for acquisition and interpretation of MRI of the spine and sacroiliac joints in the diagnosis of axial spondyloarthritis in the UK. *Rheumatology*. 2019;58:1831-1838. doi:10.1093/rheumatology/kez173
4. Day J, Patel S, Limaye V. The role of magnetic resonance imaging techniques in evaluation and management of the idiopathic inflammatory myopathies. *Semin Arthritis Rheum*. 2017;46:642-649. doi:10.1016/J.SEMARTHRIT.2016.11.001
5. Miller E, Uleryk E, Doria AS. Evidence-based outcomes of studies addressing diagnostic accuracy of MRI of juvenile idiopathic arthritis. *Am J Roentgenol*. 2012;192:1209-1218. doi:10.2214/AJR.08.2304
6. Shaban N, Hoad CL, Naim I, et al. Imaging in inflammatory bowel disease: current and future perspectives. *Frontline Gastroenterol*. 2022;13:e28-e34. doi:10.1136/FLGASTRO-2022-102117
7. Bray TJP, Bainbridge A, Punwani S, Ioannou Y, Hall-Craggs MA. Simultaneous quantification of bone edema/adiposity and structure in inflamed bone using chemical shift-encoded MRI in spondyloarthritis. *Magn Reson Med*. 2018;79:1031-1042. doi:10.1002/mrm.26729
8. Marty B, Baudin PY, Reyngoudt H, et al. Simultaneous muscle water T_2 and fat fraction mapping using transverse relaxometry with stimulated echo compensation. *NMR Biomed*. 2016;29:431-443. doi:10.1002/NBM.3459
9. Araujo ECA, Marty B, Carlier PG, Baudin P-Y, Reyngoudt H. Multiexponential analysis of the water T_2-relaxation in the skeletal muscle provides distinct markers of disease activity between inflammatory and dystrophic myopathies. *J Magn Reson Imaging*. 2021;53:181-189. doi:10.1002/JMRI.27300
10. Yuan W, Lei Y, Tang C, et al. Quantification of bone marrow edema in rheumatoid arthritis by using high-speed T_2-corrected multiecho acquisition of 1H magnetic resonance spectroscopy: a feasibility study. *Clin Rheumatol*. 2021;3:1-9. doi:10.1007/S10067-021-05764-X
11. Janiczek RL, Gambarota G, Sinclair CDJ, et al. Simultaneous T_2 and lipid quantitation using IDEAL-CPMG. *Magn Reson Med*. 2011;66:1293-1302. doi:10.1002/mrm.22916
12. Sinclair CDJ, Morrow JM, Janiczek RL, et al. Stability and sensitivity of water T_2 obtained with IDEAL-CPMG in healthy and fat-infiltrated skeletal muscle. *NMR Biomed*. 2016;29:1800-1812. doi:10.1002/nbm.3654
13. Maksymowych WP, Inman RD, Salonen D, et al. Spondyloarthritis Research Consortium of Canada magnetic resonance imaging index for assessment of sacroiliac joint inflammation in ankylosing spondylitis. *Arthritis Care Res*. 2005;53:703-709. doi:10.1002/art.21445
14. Santini F, Deligianni X, Paoletti M, et al. Fast open-source toolkit for water T_2 mapping in the presence of fat from multi-echo spin-echo acquisitions for muscle MRI. *Front Neurol*. 2021;12:248. doi:10.3389/fneur.2021.630387
15. Schlaeger S, Weidlich D, Klupp E, et al. Water T_2 mapping in fatty infiltrated thigh muscles of patients with neuromuscular diseases using a T_2 -prepared 3D turbo spin echo with SPAIR. *J Magn Reson Imaging*. 2019;51:1727-1736. doi:10.1002/jmri.27032
16. Özgen A. The value of the T_2-weighted multipoint Dixon sequence in MRI of sacroiliac joints for the diagnosis of active and chronic sacroiliitis. *Am J Roentgenol*. 2017;208:603-608. doi:10.2214/ajr.16.16774

17. Eggers H, Brendel B, Duijndam A, Herigault G. Dual-echo Dixon imaging with flexible choice of echo times. *Magn Reson Med*. 2010;65:96-107. doi:10.1002/mrm.22578
18. Snyder J, McPhee KC, Wilman AH. T_2 quantification in brain using 3D fast spin-echo imaging with long echo trains. *Magn Reson Med*. 2022;87:2145-2160. doi:10.1002/mrm.29113
19. Weigel M. Extended phase graphs: dephasing, RF pulses, and echoes-pure and simple. *J Magn Reson Imaging*. 2014;41:266-295. doi:10.1002/jmri.24619
20. Yu H, Shimakawa A, McKenzie CA, Brodsky E, Brittain JH, Reeder SB. Multiecho water-fat separation and simultaneous R_2* estimation with multifrequency fat spectrum modeling. *Magn Reson Med*. 2008;60:1122-1134. doi:10.1002/mrm.21737
21. Fatemi Y, Danyali H, Helfroush MS, Amiri H. Fast T_2 mapping using multi-echo spin-echo MRI: A linear order approach. *Magn Reson Med*. 2020;84:2815-2830. doi:10.1002/mrm.28309
22. Christoffersson JO, Olsson LE, Sjöberg S. Nickel-doped agarose gel phantoms in MR imaging. *Acta Radiol*. 1991;32:426-431. doi:10.3109/02841859109177599
23. Hines CDG, Yu H, Shimakawa A, McKenzie CA, Brittain JH, Reeder SB. T_1 independent, T_2* corrected MRI with accurate spectral modeling for quantification of fat: validation in a fat-water-SPIO phantom. *J Magn Reson Imaging*. 2009;30:1215-1222. doi:10.1002/jmri.21957
24. Özcan M, Seven S. Physical and chemical analysis and fatty acid composition of peanut, peanut oil and peanut butter from ÇOM and NC-7 cultivars. *Grasas y Aceites*. 2003;54:12-18. doi:10.3989/GYA.2003.V54.I1.270
25. Hernando D, Sharma SD, Kramer H, Reeder SB. On the confounding effect of temperature on chemical shift-encoded fat quantification. *Magn Reson Med*. 2013;72:464-470. doi:10.1002/mrm.24951
26. Vanhamme L, van den Boogaart A, Van Huffel S. Improved method for accurate and efficient quantification of MRS data with use of prior knowledge. *J Magn Reson*. 1997;129:35-43. doi:10.1006/jmre.1997.1244
27. Naressi A, Couturier C, Castang I, De Beer R, Graveron-Demilly D. Java-based graphical user interface for MRUI, a software package for quantitation of in vivo/medical magnetic resonance spectroscopy signals. *Comput Biol Med*. 2001;31:269-286. doi:10.1016/S0010-4825(01)00006-3
28. Stefan D, Di Cesare F, Andrasescu A, et al. Quantitation of magnetic resonance spectroscopy signals: The jMRUI software package. *Meas Sci Technol*. 2009;20:104035. doi:10.1088/0957-0233/20/10/104035
29. Hamilton G, Yokoo T, Bydder M, et al. In vivo characterization of the liver fat1H MR spectrum. *NMR in Biomed*. 2010;24:784-790. doi:10.1002/nbm.1622
30. Kim D, Jensen JH, Wu EX, Sheth SS, Brittenham GM. Breath-hold multiecho fast spin-echo pulse sequence for accurate R2 measurement in the heart and liver. *Magn Reson Med*. 2009;62:300-306. doi:10.1002/mrm.22047
31. Nöth U, Shrestha M, Schüre JR, Deichmann R. Quantitative in vivo T_2 mapping using fast spin echo techniques—a linear correction procedure. *Neuroimage*. 2017;157:476-485. doi:10.1016/j.neuroimage.2017.06.017
32. Lebel RM, Wilman AH. Transverse relaxometry with stimulated echo compensation. *Magn Reson Med*. 2010;64:1005-1014. doi:10.1002/mrm.22487
33. Zur Y. An algorithm to calculate the NMR signal of a multi spin-echo sequence with relaxation and spin-diffusion. *J Magn Reson*. 2004;171:97-106. doi:10.1016/j.jmr.2004.07.018
34. Prasloski T, Mädler B, Xiang Q-S, MacKay A, Jones C. Applications of stimulated echo correction to multicomponent T_2 analysis. *Magn Reson Med*. 2011;67:1803-1814. doi:10.1002/mrm.23157
35. Ben-Eliezer N, Sodickson DK, Block KT. Rapid and accurate T_2 mapping from multi-spin-echo data using Bloch-simulation-based reconstruction. *Magn Reson Med*. 2014;73:809-817. doi:10.1002/mrm.25156
36. Neumann D, Blaimer M, Jakob PM, Breuer FA. Simple recipe for accurate T_2 quantification with multi spin-echo acquisitions. *Magn Reson Mater Phys Biol Med*. 2014;27:567-577. doi:10.1007/s10334-014-0438-3
37. Huang C, Altbach MI, El Fakhri G. Pattern recognition for rapid T_2 mapping with stimulated echo compensation. *Magn Reson Imaging*. 2014;32:969-974. doi:10.1016/j.mri.2014.04.014
38. Ostenson J, Damon BM, Welch EB. MR fingerprinting with simultaneous T_1, T_2, and fat signal fraction estimation with integrated B_0 correction reduces bias in water T_1 and T_2 estimates. *Magn Reson Imaging*. 2019;60:7-19. doi:10.1016/j.mri.2019.03.017
39. Jaubert O, Cruz G, Bustin A, et al. Water–fat Dixon cardiac magnetic resonance fingerprinting. *Magn Reson Med*. 2019;83:2107-2123. doi:10.1002/mrm.28070

SUPPORTING INFORMATION

Additional supporting information may be found in the online version of the article at the publisher's website.

Figure S1. Slice from multislice acquisition panel, demonstrating almost identical image contrast and quality to the single-slice acquisition in Figure 8.

Figure S2. Multiple slices from the multislice acquisition, demonstrating that the image quality is consistent throughout the whole volume.

How to cite this article: Gollifer RM, Bray TJP, Kruezi A, et al. A multiparametric alternative to short inversion-time inversion recovery for imaging inflammation: T_{2water} and fat fraction measurement using chemical shift–encoded turbo spin-echo MRI. *Magn Reson Med*. 2023;90:1010-1024. doi: 10.1002/mrm.29689